

Original article

Use of controlled fractures in enhanced geothermal systems

Harun U. Rashid, Olufemi Olorode[✉]*

Department of Petroleum Engineering, Louisiana State University, Baton Rouge, Louisiana 70803, United States

Keywords:

Enhanced geothermal systems technology
slot-drill fractures
fractured horizontal wells
coupled heat and fluid flow
explicit fracture model

Cited as:

Rashid, H. U., Olorode, O. Use of controlled fractures in enhanced geothermal systems. *Advances in Geo-Energy Research*, 2024, 12(1): 35-51. <https://doi.org/10.46690/ager.2024.04.04>

Abstract:

Enhanced geothermal systems are typically tight and naturally fractured like unconventional oil and gas reservoirs, so the leading technology being evaluated for their commercial development is also multistage fractured horizontal wells. The state-of-the-art approach of thermal recovery from enhanced geothermal systems involves injecting cold water into a multiply fractured horizontal/deviated well and producing hot water from a parallel well above the injector. The limited control over the hydraulic fracture location, size, and orientation in multistage fractured horizontal wells results in low and unpredictable thermal recoveries. To this end, we present an alternative technology that employs unique configurations of mechanically cut fractures to recover heat efficiently from all parts of hot rocks in the subsurface. The precise control over these fractures' location, size, orientation, and conductivity facilitates the design of suitable configurations of intersecting fractures. This paper presents high-resolution numerical studies of thermal recovery from both multistage fractured horizontal wells and the proposed approach. The results show that the proposed approach can recover significantly more thermal energy than multistage fractured horizontal wells. Additionally, the temperature profiles show that precise control over the location of the fractures allows the reliable and efficient recovery of heat from all parts of the enhanced geothermal systems, which could be the key to their commercial development.

1. Introduction

Enhanced or engineered geothermal systems (EGS) are subsurface heat exchange systems created by fracturing low-matrix permeability hot rocks. The idea is to extract thermal energy economically by circulating cold water through these typically fractured rocks and producing the water after it has been heated via contact with the hot rock in a so-called closed loop (Tester et al., 2006). Although early research on EGS development focused on the hydraulic fracturing of vertical wells, several researchers have evaluated the idea of shearing existing joints or natural fractures (NFs) in these hot rocks (Batchelor, 1977). Unfortunately, these approaches have yet to prove commercially viable. The sketch in Fig. 1 illustrates how the multistage hydraulic fracturing technology is applied to EGS. The process (as implemented in the Utah FORGE) involves first drilling a horizontal injection well, and hydraulically fracturing it in multiple stages by pumping slick water at pressures above the least principal stress of

the formation. A horizontal production well is then drilled vertically above the fractured injection well to intersect all 3 hydraulic fractures, as shown in the figure below. Cold water is then injected continuously into the hot rock through the injection well, while the heated water is produced from the production well. Various authors indicate that a reasonable investment in research and development of EGS in the USA could provide over 100 electric Gigawatts (at a competitive cost) in the next 50 years (Tester et al., 2006; Aghahosseini and Breyer, 2020). The global market for EGS is estimated to be worth \$1.8 billion and \$3.7 billion in 2020 and 2030, respectively (<https://www.reportlinker.com/p06219256>). This has fueled a surge in DOE funding for geothermal resources in the last couple of years, and the trend is expected to continue. One such funded geothermal research project is the Utah FORGE project (<https://utahforge.com>), which is currently evaluating the first commercial development of EGS with multistage fractured horizontal wells (MFHW). The idea of using MFHW is based on its success in the commercial de-

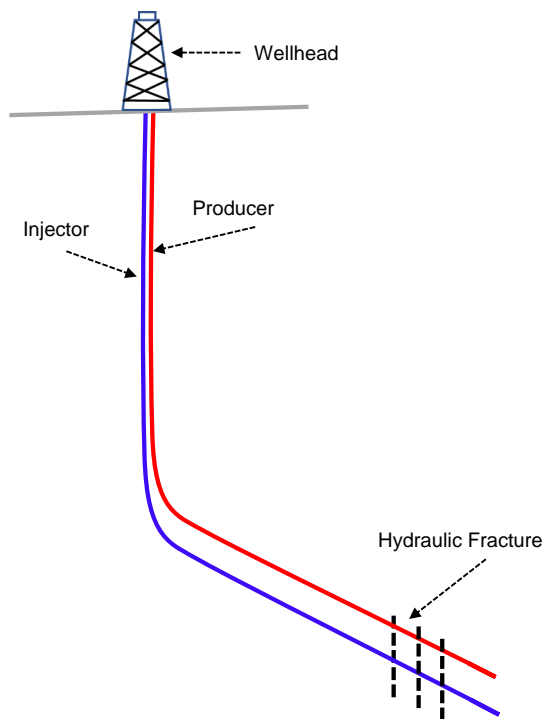


Fig. 1. Illustration of heat extraction from EGS using MFHW.

development of unconventional oil and gas reservoirs, which are also low-permeability matrix systems.

Considering the high costs of evaluating different EGS technologies in the field, several researchers have developed coupled heat and fluid flow simulators to simulate the performance of these technologies. Several researchers have designed computer experiments and sensitivity studies using these simulators to evaluate the potential of MFHW in EGS. For instance, Asai et al. (2018) and Gong et al. (2020) performed numerical simulation studies that showed that horizontal wells have higher efficiency than vertical hydraulically fractured wells, which indicates the possible success of MFHW in EGS.

Although virtually all published numerical studies of the application of MFHW in EGS assume that the horizontal injection and production wells intersect all the hydraulic fractures, which are planar and bi-wing, this is only an unrealistic idealization. The negligible control over the size and orientation of hydraulic fractures, as well as the non-planarity and non-orthogonality of these fractures, will result in a lower heat recovery in the field compared to the simulated recovery. The expected lower recovery from non-planar and non-orthogonal fractures (compared to planar and orthogonal fractures) is demonstrated in an analogous system for the primary production from unconventional gas reservoirs (Olorode et al., 2013). These uncertainties in MFHW highlight the need for a controlled fracture system that can be used to recover heat reliably and efficiently from all parts of an EGS.

EGS are typically naturally fractured and have low matrix permeability like unconventional oil and gas reservoirs, so the fractures generally are modeled using similar methods. As explained in Olorode et al. (2021), the effective models represent the fractured reservoir as an effective medium with

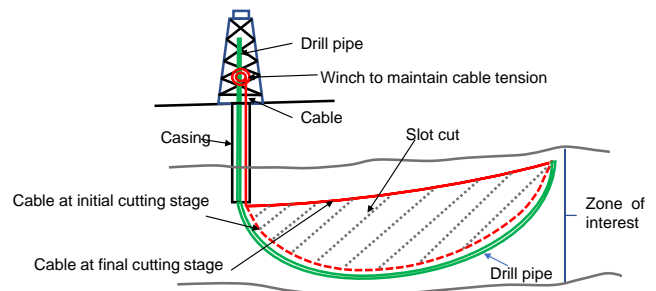


Fig. 2. Illustration of how to cut mechanical fractures using a tensioned cable, as presented in Carter (2009).

homogenized or average properties. For example, Rashid et al. (2018) homogenized the naturally fractured system into a single-porosity system to simulate an EGS. Other multiple continuum formulations of the effective medium include the dual-porosity (Warren and Root, 1963), dual-permeability (Gilman and Kazemi, 1983), and multi-continuum models (Pruess and Narasimhan, 1982; March et al., 2021).

Unlike the effective medium models, discrete models individually account for each fracture in fractured reservoirs. These include the discrete fracture model (Kim and Deo, 2000; Karimi-Fard et al., 2004; Klemetsdal et al., 2023), embedded discrete fracture model (Li and Lee, 2008; Wong et al., 2021), and projection-based embedded discrete fracture model (pEDFM) (Tene et al., 2017; Olorode et al., 2020, 2021; Rao et al., 2022). Although pEDFM was developed to model NFs of high and low conductivity, it cannot accurately model low-conductivity fractures that neither lie parallel to any of the spatial (x -, y -, and z -) axes nor cut through the diagonals of the matrix cells (Rao and Liu, 2022; Rashid and Olorode, 2024). To obtain reference solutions for the EGS systems studied, the fully dimensional (or explicit fracture) model was used, where each natural fracture is meshed in three-dimensional and partitioned into several fracture cells. Although this approach is very computationally expensive, it is the most accurate approach to model fractured reservoirs. The idea is to obtain high-resolution reference solutions, which can be used to validate the application of other fracture models.

The next section presents our proposed approach to recover heat from EGS using controlled fractures, which are mechanically cut into the rock with the slot-drilling technology proposed by Carter (2009).

2. Proposed slot-drill EGS

This section presents our design of slot-drill (SD) fracture configurations that can lead to improved, reliable, and efficient heat recovery from all parts of an EGS. The SD technology is based on ideas involving using a chain cutter that is pulled through massive rock outcrops, as in Hurd (1980) and Farrar et al. (1991). The EGS approach proposed here involves designing an interconnected system of fractures, which are mechanically cut using the SD technology (Carter, 2009). The proposed application of this concept to cut fractures in the subsurface involves using a deviated well bore, as shown in Fig. 2.

A flexible and tensioned cutting cable (shown as the curved



Fig. 3. Demonstration of formation cutting using steel abrasive cable (Carter, 2009).

red lines) is then inserted into the wellbore and fixed at the toe of the wellbore. The back-and-forth motion of the tensioned cable could result in the cutting of the SD fracture (SDF), shown as the shaded semi-circle in the Fig. 3. Although the sketch shows a somewhat fictitious representation of the SDF, we are working on several modifications of the original slot-drilling technique of (Carter, 2009), which will be a subject of a future publication. The idea is to create a modified and more feasible approach to cut the harder rocks expected in geothermal reservoirs mechanically. However, this paper focuses on the simulation of different configurations of these mechanically cut fractures that can lead to more efficient and reliable EGS that can recover evenly from all parts of fractured or unfractured hot rocks in the subsurface. Several researchers have already presented a numerical study of the successful application of slot drill fracture in enhanced oil recovery (Ogunwole, 2012; Amer and Olorode, 2022). This study presents the first numerical evaluation of slot drill fracture into enhanced geothermal systems. Also, the configuration of fractures and the completion technology proposed in the study are noble and efficient.

Carter Jr (2017) proposed the use of a single well to cut multiple fractures in different directions (azimuths) from a single location, as shown in Fig. 4. This work extends this idea by proposing intersecting SDFs drilled from different wells, as shown in Fig. 5. As shown in this figure, two different SDF configurations are proposed, which are referred to as the eight SDF triplet and six SDF doublet configurations, respectively. Although, only eight and six SDFs are shown, the actual implementation in the subsurface will involve repeating the pattern of alternating injector and producer as many times as needed.

2.1 Eight SDF triplets

This configuration is so-called because the pattern contains eight SDFs and three wells, as shown in Fig. 5(a). Here, a water injection well (shown in green) is surrounded by two producers (in red). It is easy to observe that each vertical well section (whether for a producer or injector) can be deviated and drilled in four different directions. For example, the four SDFs that intersect the injector well in the middle of the domain in Fig. 5(a) can be created by drilling four different deviated wellbores from the injector.

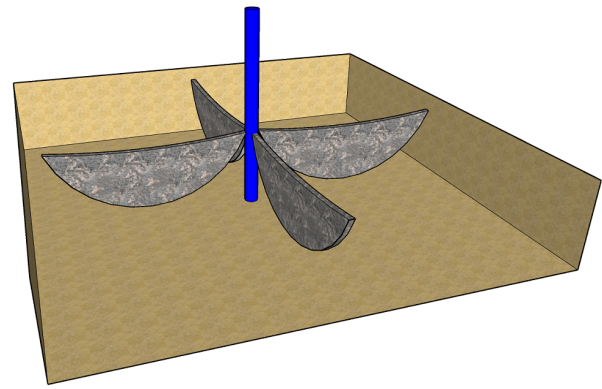


Fig. 4. Illustration of the approach to cut multiple fractures from one well (modified from Carter (2009)).

2.2 Six SDF doublet

This configuration is so-called because the repeating pattern contains six SDFs and two wells, as shown in Figs. 5(b) and 5(c). Fig. 5(b) involves flowing the fluid in parallel, whereas, in Fig. 5(c), the well will be completed such that it only injects water into the outermost (either right-most or left-most) fracture. If the injector is restricted to inject only into the right-most SDF (SDF #1), for example, the producer will be restricted to only produce from the left-most fracture (SDF #6). The idea is that the fluid will need to move through the fractures in ascending order from SDF #1 through #6. The connection between specific SDFs like SDF #2 and #3 can be isolated from the tubing and other SDFs using packers in the annulus, which is only open in the sector or region where those two fractures intersect the annulus. However, SDF #6 will be the only SDF allowed to flow into the tubing.

The doublet configuration with parallel flow is referred to as the “doublet parallel” case, whereas the other doublet configuration is referred to as the “doublet series” case. The former was introduced because our numerical simulation studies reveal that although the thermal recoveries of both cases were approximately equal, the latter required unrealistically high injection pressures to flow fluids through the fracture and obtain the same pressure in the production well. Therefore, all subsequent references to the doublet case in this work refer to the doublet parallel configuration. Figs. S1 and S2 in the Supplementary Material provided with this paper show the comparison of the doublet parallel and series configurations for the 6 and 14 SDF cases, respectively.

Compared to the SD triplet configuration, the SD doublet design is more flexible regarding the number of fractures that can be placed in any given area and requires fewer wells per unit SDF and per unit area. For instance, it is easy to see that the same vertical injection well section at the bottom corner of the domain can be used to drill the SDFs in the next pattern below and to the left of the current pattern shown in Fig. 5(b). Additionally, to compare this configuration with a MFHW of a much larger total fracture area, Section 5 shows a simulation of a fourteen-SDF doublet configuration.

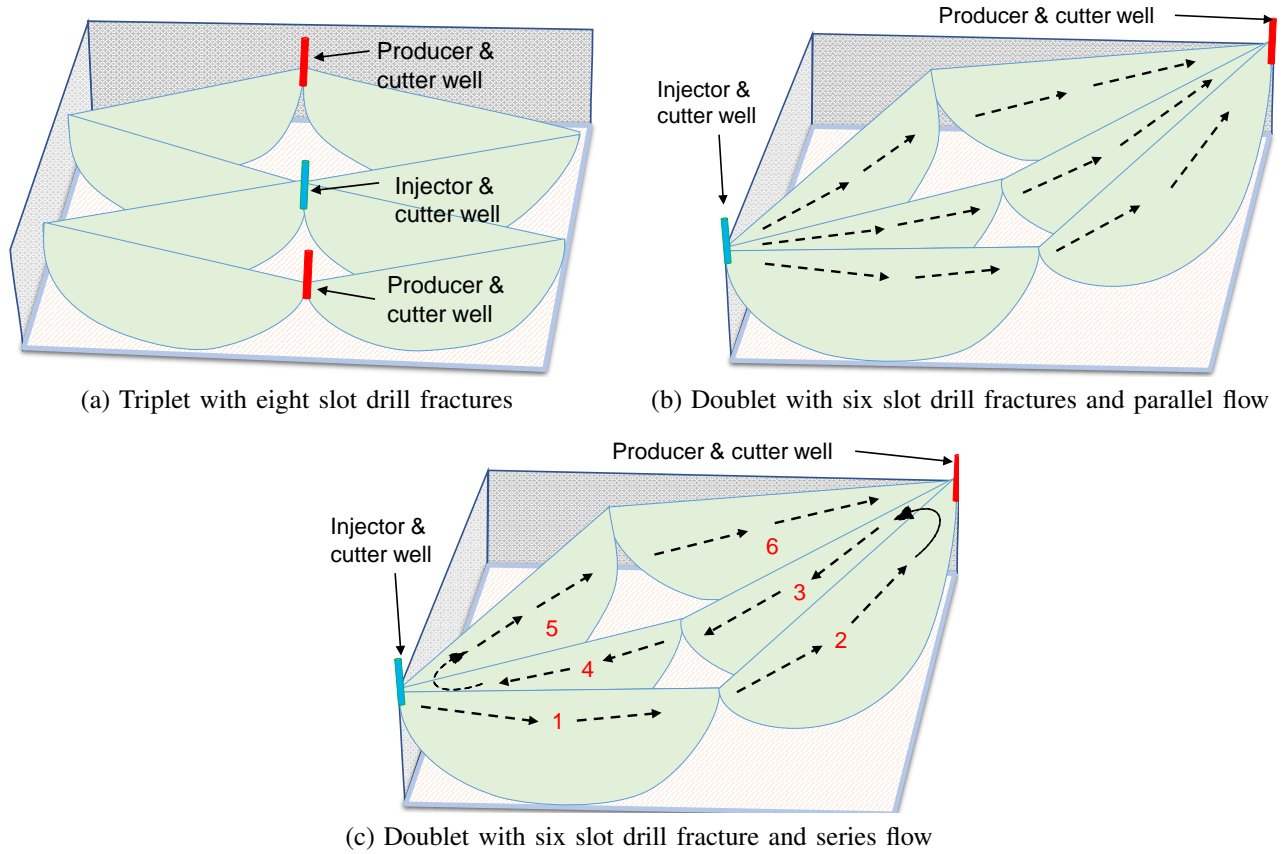


Fig. 5. Illustration of SD EGS.

3. Governing equations

Modelling the coupled flow of fluid and heat in geothermal reservoirs involves solving the equations that govern both the fluid flow and heat flow. The mass conservation equation for single-phase fluid flow in porous media can be written as follows:

$$\partial_t(\phi\rho_f) + \nabla(\rho_f\vec{v}_f) = \frac{\rho_f q}{V} \quad (1)$$

where ϕ is the porosity of the rock, ρ_f is the fluid density, \vec{v}_f is the Darcy velocity of the fluid, q is the source or sink, and V is the bulk volume. From the Darcy equation, the Darcy velocity is given as:

$$\vec{v}_f = -\frac{\mathbf{K}}{\mu_f}(\nabla p - \rho_f g \nabla z) \quad (2)$$

where \mathbf{K} is the permeability, μ_f is the fluid viscosity, z is the depth, p is the pressure, and g is the acceleration due to gravity.

The energy conservation equation governs the flow of heat in geothermal reservoirs. It is written as follows:

$$\partial_t[\phi_f \rho_f C_f T + (1 - \phi) \rho_r C_r T] + \nabla(\rho_f \vec{v}_f h_f) + \nabla(\vec{H}_f + \vec{H}_r) = Q_f h_f \quad (3)$$

where T is the current temperature of the system, ρ_r is the rock density, ϕ_f is the fracture porosity, while C_f and C_r are the specific heat capacities of the fluid and rock, respectively.

The term $Q_f h_f$ is the energy source or sink term, and h_f is the specific enthalpy, which is given as:

$$h_f = C_f \Delta T + \frac{p}{\rho_f} \quad (4)$$

The H_f and H_r terms in Eq. (3) represent the heat conduction for the fluid and rock, respectively. The equation for heat conduction is given by Fourier's law:

$$\vec{H}_f = -\phi \lambda_f \nabla T \quad (5)$$

$$\vec{H}_r = -(1 - \phi) \lambda_r \nabla T \quad (6)$$

where λ_f and λ_r represent the thermal conductivity of the fluid and rock, respectively.

Solving the governing mass and energy conservation equations involves discretizing them with respect to time using the implicit or backward Euler scheme. This yields the semi-discrete form of the energy balance equation:

$$\frac{[\phi_f \rho_f C_f T + (1 - \phi) \rho_r C_r T]^{n+1} - [\phi_f \rho_f C_f T + (1 - \phi) \rho_r C_r T]^n}{\Delta t} + \nabla[\rho_f \vec{v}_f h_f]^{n+1} + \nabla[\vec{H}_f + \vec{H}_r]^{n+1} - [Q_f h_f]^{n+1} = R_e^{n+1} \quad (7)$$

Similarly, the semi-discrete form of the mass-conservation equation is given as:

$$\frac{[\phi \rho_f]^{n+1} - [\phi \rho_f]^n}{\Delta t} + \nabla[\rho_f \vec{v}_f]^{n+1} - \left[\frac{\rho_f q}{V}\right]^{n+1} = R_m^{n+1} \quad (8)$$

where R_e^{n+1} and R_m^{n+1} refer to the residual of the energy and mass balance equations, respectively.

This work uses the finite-volume discretization with single-point upwind weighting for spatial discretization, as in Collignon et al. (2021). The discrete divergence and gradient operators are used to simplify the numerical implementation of the spatial discretization, as discussed in Section 4.4 of Lie (2019).

These coupled nonlinear equations are linearized using the Newton-Raphson iteration scheme. The linearized system of equations is then solved for the changes in the primary variables (ΔX) at each Newton iteration, using a Bi-Conjugate Gradient Stabilized linear solver with an Algebraic Multi-Grid pre-conditioner. The changes in the primary variables are then added to the previous values of the primary variables (X), and the procedure is repeated until the system converges. Upon convergence, the solution algorithm proceeds to the next time step and repeats this Newton iteration.

To perform the simulation studies presented in this paper, we used the geothermal (Collignon et al., 2020, 2021) and unstructured gridding (Berge et al., 2019, 2021) modules in the MATLAB Reservoir Simulation Toolbox (MRST) (Lie, 2019; Lie and Møyner, 2021). The stochastic NFs simulated were created using the Alghalandis Discrete Fracture Network Engineering code, which is presented in Alghalandis (2018).

3.1 Thermal recovery fraction

This work uses the thermal recovery fraction defined in Tester et al. (2006) to facilitate a reasonable comparison between the thermal energy recovered from different simulation cases. The equation for the thermal recovery fraction (RF) can be given as follows:

$$RF = \frac{Q_r}{Q_t} \quad (9)$$

where Q_r is the recoverable energy from a geothermal reservoir, which is given as:

$$Q_r = \rho_r V_a C_r (T_{r,i} - T_{r,a}) \quad (10)$$

and Q_t is the total energy stored in the reservoir, which is given as:

$$Q_t = \rho_r V_t C_r (T_{r,i} - T_o) \quad (11)$$

In these equations, V_a is the active or effective reservoir volume, V_t is the total reservoir volume, C_r is the specific heat capacity of the rock, $T_{r,i}$ is the mean initial reservoir temperature, $T_{r,a}$ is the mean reservoir temperature at abandonment, and T_o is the ambient temperature. It is worth noting that Eqs. (10) and (11) implicitly homogenize the entire reservoir and calculate the energy stored from mean reservoir properties. However, in the numerical studies performed in this work, each grid block or cell in the simulation domain has unique temperatures, density, bulk volume, etc. So, the recovery factor is calculated from the summation of the energy stored in each cell at the initial condition and at the end of the simulation. Therefore, the recovery factor (RF) is computed as follows:

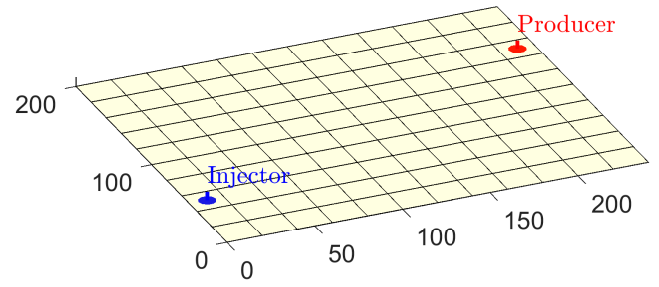


Fig. 6. Simulation domain for a simple injector and producer well pair in a 2D Cartesian grid.

$$RF = \frac{\sum_{j=1}^{n_c} \rho_r V_g^j C_r (T_{r,i} - T_r^j)}{\sum_{j=1}^{n_c} \rho_r V_{g,i}^j C_r (T_{r,i} - T_o)} \quad (12)$$

where V_g^j represents the grain volume in cell j at any pressure and temperature (which is the product of the cell volume and one minus the current porosity of the cell), $V_{g,i}^j$ is the initial value of the grain volume in cell j , and T_r^j is the current temperature in cell j . The superscript n_c in the summation indicates that the equation is evaluated and summed over the total number of cells (n_c) in the simulation domain.

3.2 Thermal energy

Estimating the thermal energy of the produced hot water is essential for evaluating the commercial feasibility of an enhanced geothermal system. The "extractable" thermal energy depends on the produced fluid's amount and temperature. To estimate it, we first compute the extractable energy at the wellhead (E_{wh}) as in Franco and Donatini (2017):

$$E_{wh} = m_{wh} (h_{wh} - h_{ref}) \quad (13)$$

where h_{wh} and h_{ref} are the enthalpies of the fluid at the wellhead and reference conditions, respectively. The symbol m_{wh} represents the mass of hot water extracted from the producer. The mass flow rate (\dot{m}_{wh}) can be calculated as follows:

$$\dot{m}_{wh} = \rho q_1 \quad (14)$$

where q_1 is the volumetric flow rate at the wellhead. Therefore, we can estimate the cumulative thermal energy (E_{cum}) by integrating the product of the mass flow rate Eq. (14) and $(h_{wh} - h_{ref})$ over a time interval (dt) in seconds:

$$E_{cum} = \int \dot{m}_{wh} (h_{wh} - h_{ref}) dt \quad (15)$$

4. Validation against TOUGH3

This section verifies our MRST simulations against the TOUGH3 simulator from the Lawrence Berkeley National Lab (Jung et al., 2021). Fig. 6 presents the simulation domain used. The problem involves injecting water at 22 °C close to the bottom left of the domain, while hot water is produced from the well close to the top right of the domain. To ensure that the same mesh is used in TOUGH3 and our modified MRST code, we wrote a MATLAB script that exports the MRST mesh dire-

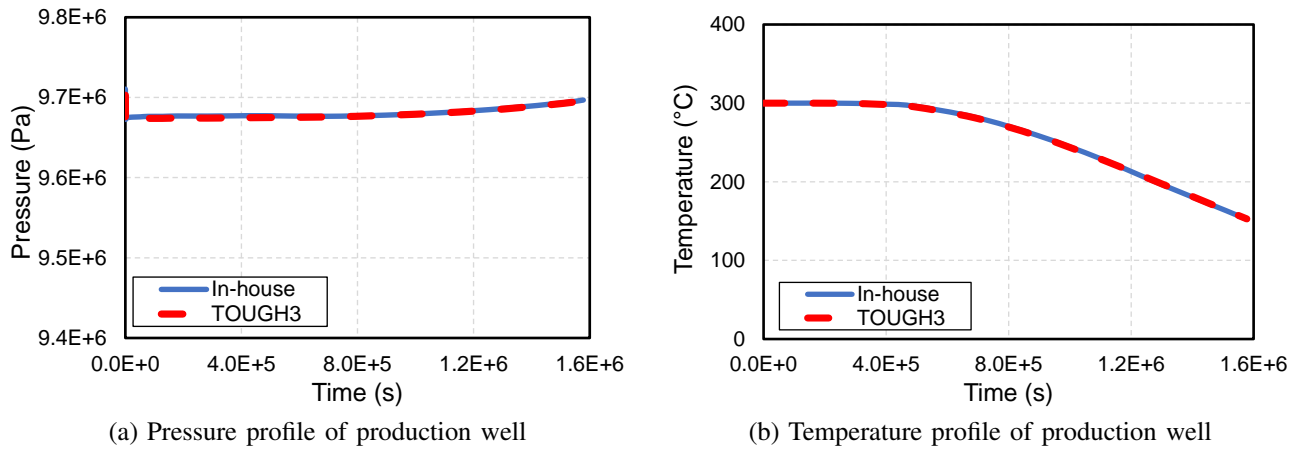


Fig. 7. Validation of model against TOUGH3 shows a good match.

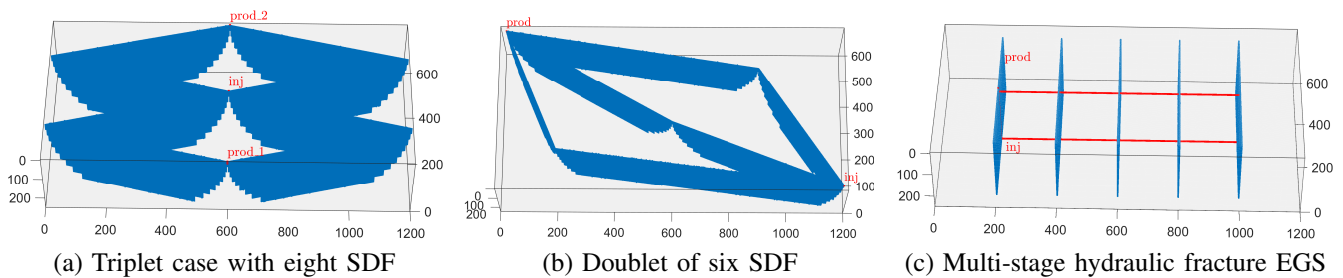


Fig. 8. Simulation domains for the coupled thermal and hydraulic simulation.

Table 1. Parameters used for the validation against TOUGH3.

Parameters	Value	Unit
Permeability	2e-10	m ²
Porosity	0.5	/
Reservoir dimensions	240 × 200 × 0.04	m ³
Grid dimensions	20 × 20 × 0.04	m ³
Initial reservoir pressure	9.8e6	Pa
Initial reservoir temperature	300	K
Fluid thermal conductivity	0.6	W/(m·K)
Fluid heat capacity	4,200	J/(Kg·K)
Fluid density	1,000	Kg/m ³
Fluid viscosity	1e-3	Pa·s
Rock thermal conductivity	2,650	W/(m·K)
Rock heat capacity	1,000	J/(Kg·K)
Rock density	2,650	Kg/m ³
Injection rate	1e-3	m ³ /s
Bottom hole pressure	9.65e6	Pa

ctly into the TOUGH3 mesh input format. Table 1 summarizes the model parameters for this verification case.

Fig. 7 presents the plot of the producer's pressure and

temperature over 18 days. The maximum errors in pressure and temperature are 0.08% and 0.45%, respectively. These results show that our model closely matches the TOUGH3 code over the simulated period of injection and production. The results show that the pressure of the production well increases almost instantaneously to a value of 9.67 MPa, and slowly increases to 9.7 MPa. In contrast, the temperature of the producer gradually declines from the initial temperature of 300 °C to a final value of 153 °C.

5. Application of SDFs in EGS

This section presents the simulation studies of the SDF EGS configurations shown in Section 2. Fig. 8 gives the mesh for the SD EGS triplet (in Fig. 8(a)), SD EGS doublet (Fig. 8(b)), and an MFHW case (Fig. 8(c)) with the same total fracture surface area as the SD EGS cases. The same reservoir dimensions were used in all three cases to reasonably compare the simulated thermal recovery fraction of the proposed SD EGS technologies and the state-of-the-art approach, which uses MFHW. The configuration of the MFHW case is consistent with the proposed approach for the development of the Utah FORGE project, where the bottom horizontal or deviated well is used to inject cold water, and a relatively parallel well above the injector is used to produce the hot water. Table 2 outlines the model parameters used in the simulation of the three cases presented. Although all the simulation results presented used no-flow and fully insulated boundary conditions on the external faces of the simulation

Table 2. Model parameters used in the comparative study of the geothermal potential of the MFHW and SD EGS cases.

Parameters	Value	Unit
Matrix permeability	9.86e-21	m ²
Matrix porosity	0.01	/
Fracture permeability	9.8692e-13	m ²
Fracture porosity	0.5	/
Fracture aperture	0.05	m
Total fracture volume	2.75e6	m ³
Reservoir dimensions	1,200×600×250	m ³
Initial reservoir pressure	3e7	Pa
Initial reservoir temperature	496	K
Injected fluid temperature	293	K
Constant injection rate	0.069	m ³ /s
Constant producer bhp	2.5e7	Pa
Rock thermal conductivity	3	W/(m·K)
Rock density	2,700	Kg/m ³
Heat capacity	1,000	J/(Kg·K)
Fluid thermal conductivity	0.6	W/(m·K)
Fluid heat capacity	4,200	J/(Kg·K)
Coefficient of thermal expansion	2.07e-4	K ⁻¹
Fluid compressibility	4.4e-10	Pa ⁻¹
Fluid density	1,000	Kg/m ³
Fluid viscosity	5e-4	Pa·s

domain, Section S3 of the supplementary material shows that using constant-temperature boundary conditions does not change the trends in the results.

Fig. 9 presents the performance plots for the MFHW and SD EGS cases. These cases are compared in terms of the cumulative thermal energy of the hot water produced (in Fig. 9(a)), the temperature of the produced fluid (in Fig. 9(b)), and the thermal recovery fraction (in Fig. 9(c)). Fig. 9(a) shows that the two SDF cases yield higher cumulative thermal energy than the MFHW case. The equations presented in Section 3.2 show that the cumulative thermal energy is a linear function of enthalpy, which is a linear function of the produced temperature. So, the higher cumulative thermal energy of the SDF cases is expected because the same volume of water is injected and produced in all three cases. Still, the temperature of the produced fluid is higher in the SDF cases than in the MFHW case (as shown in Fig. 9(b)).

The temperature of the produced fluid needs to be above the commercial limit to produce electricity from an EGS. When the 20 °C (or 293.15 K) injected fluid comes in contact with the hot rock, it extracts heat from the rock, increasing the fluid temperature. For a specific amount of fluid, the temperature of the produced fluid will increase with an increase in the contact area and duration of the fluid in the subsurface. Fig. 9(b) shows that the produced fluid temperature

is highest in the SDF cases. This is expected, considering that the injected fluid travels much longer distances in the SDF cases than in the MFHW case. These longer flow paths result in larger contact areas for the injected fluid and a longer duration that the injected fluid spends in the subsurface before being produced.

Fig. 9(c) shows that the simulated thermal recovery fraction of the proposed SDF EGS cases is much higher than that of the MFHW of the same fracture area. The thermal recovery fraction for the eight SDF triplet, six SDF doublet, and the five MFHW cases are 38%, 34%, and 20%, respectively. These results imply that the proposed application of the SD technology to enhanced geothermal systems could yield a thermal recovery that is two times that of the current state-of-the-art technology, which uses MFHW.

The cumulative thermal energy and produced fluid temperature profiles of the two SDF cases are almost identical, but the thermal recovery fraction of the eight SDF triplet is higher than that for the six SDF doublet configuration. To understand this counterintuitive observation, it is worth noting that both cases produce the same total fluid volume at almost identical temperatures, and the fracture volumes for both cases are approximately the same (within 0.28%). However, the triplet case has two producers, while the doublet case has only one producer. The average temperatures (after 50 years

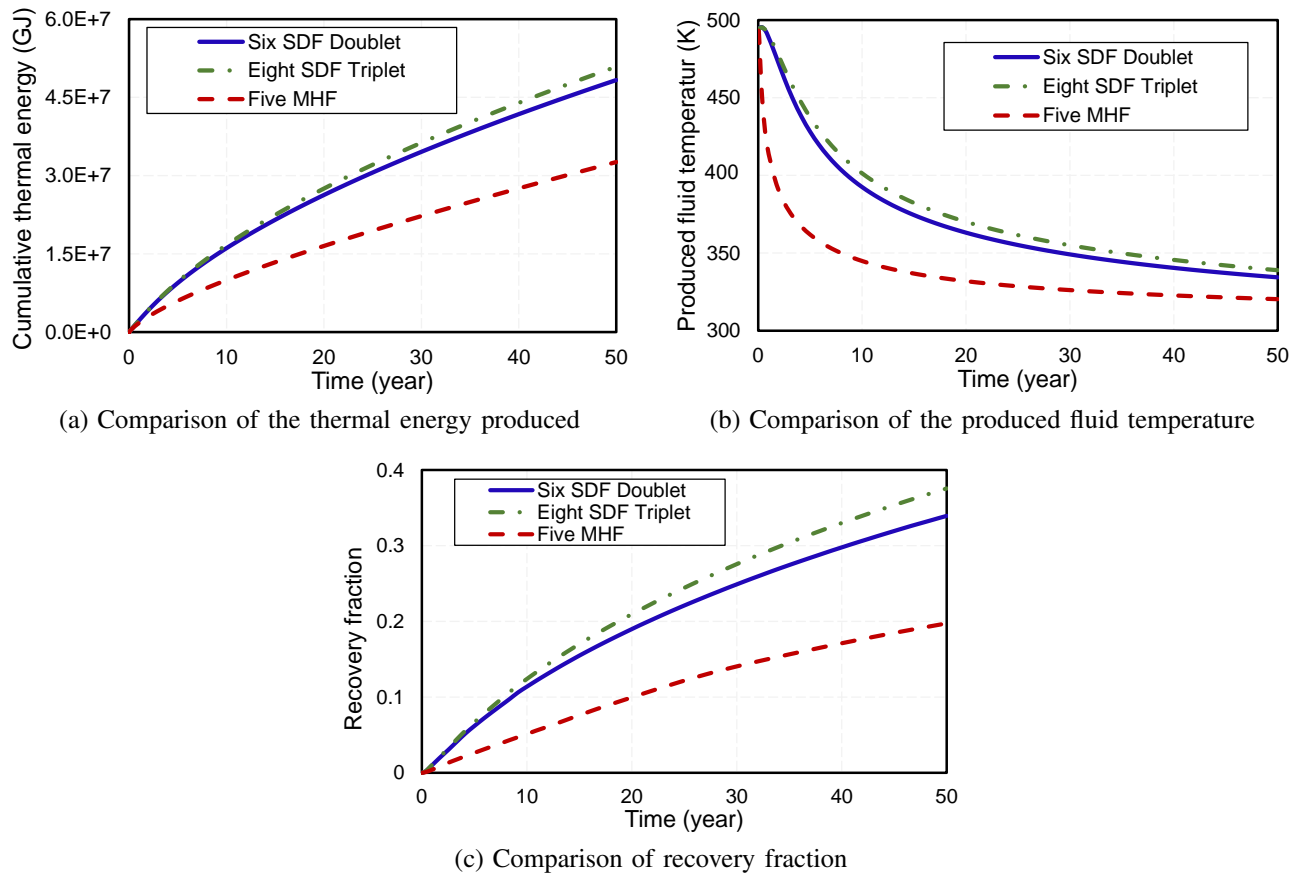


Fig. 9. Performance plots for coupled hydro-thermal simulation of the Triplet with eight SDF, doublet of six SDF, and MFHW EGS cases.

of simulated production) are 427 and 421 K for the doublet and triplet cases, respectively.

Although the temperature of the injection well is approximately the same in the two SDF cases, the production well temperature (shown in Fig. 9(b)) is observed at only one point in the reservoir for the doublet case but observed at two points in the triplet case. This production temperature is lower than the initial temperature. So, having the temperature maintained at a low value at two points yields a lower average temperature in the SDF triplet case. Unlike the cumulative thermal energy, the thermal recovery fraction is computed only from the drop in the temperature in the reservoir relative to the initial condition, as shown in Eq. (12), so the triplet case has a higher thermal recovery fraction. Although this result looks counterintuitive when compared to routine reservoir fluid production, the main difference is that the recovery fraction for fluids is computed from a ratio of fluid volumes and not a ratio of pressures, which are the corresponding primary variables.

A computation of the volume-weighted average temperature for the two SDF cases after 50 years of thermal recovery confirms that the thermal recovery fraction is indeed higher in the eight SDF triplet configuration. This yielded average temperatures of 422 and 427 K for the eight SDF triplet and six SDF doublet configurations, respectively. The lower value of the eight SDF triplet configuration indicates that more thermal

energy has been recovered from the geothermal reservoir. Additionally, this higher recovery fraction is consistent with the fact that the SDF triplet case will incur more drilling and completion costs (involving three wells) than the SDF doublet, which applies only two wells for the same reservoir domain.

To obtain insights into the thermal recovery from the three EGS configurations presented, the temperature profiles (after the simulated 50 years of thermal energy recovery) are presented in Fig. 10. The blue-colored region corresponds to the injected fluid temperature of 20 °C or 293.15 K. In contrast, the red-colored region corresponds to the portion of the reservoir that has not been recovered and is at the initial volume-weighted average temperature of 496 K. So, these temperature profiles show that a more significant portion of the reservoir rock is cooled down to the injected fluid temperature in the SDF cases when compared to the MFHW case.

5.1 Extended SDF doublet

As explained in Section 2.2, the six SDF doublet configuration uses fewer wells per unit SDF and provides the flexibility needed to use any number of SDFs within a given area. In this section, the number of SDFs (in the same domain presented in the previous section) is increased from six SDFs in the doublet configuration to 14. The idea is to evaluate the corresponding increase in thermal energy recovery as the

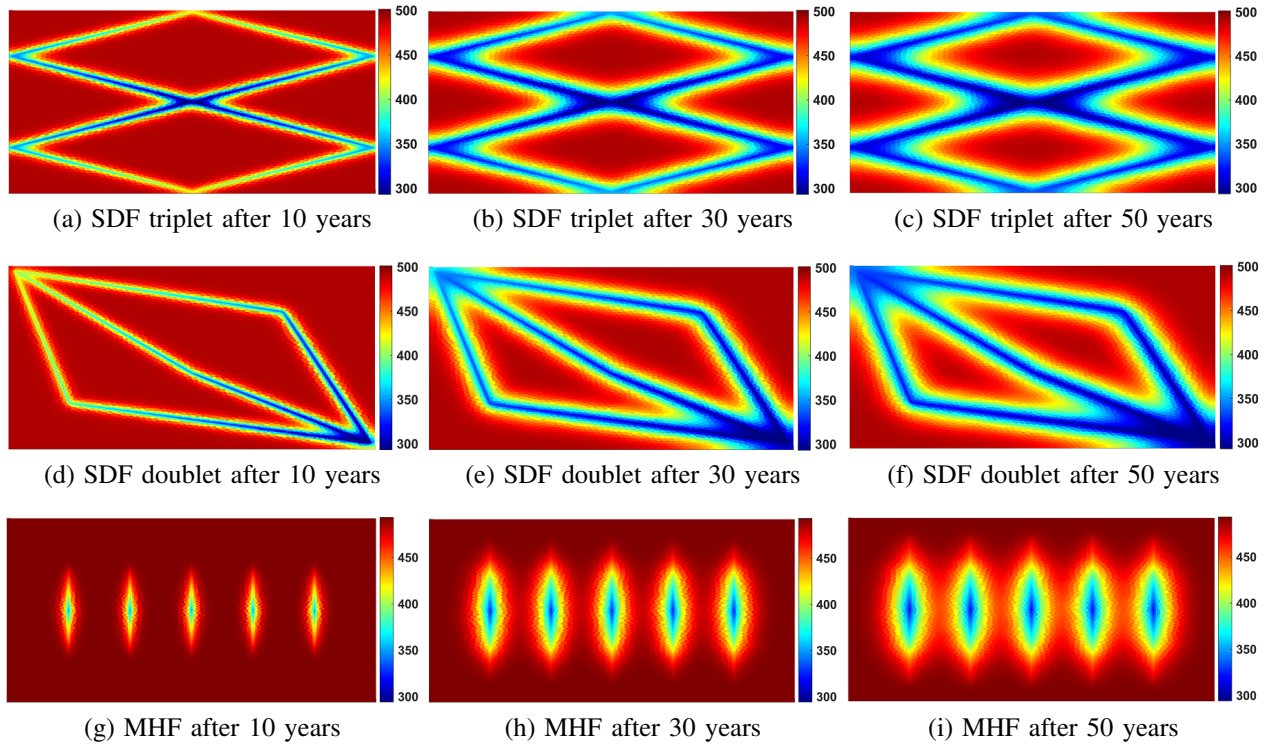


Fig. 10. These profiles show the evolution of temperature distribution at the top of the reservoir after 10, 30, and 50 years.

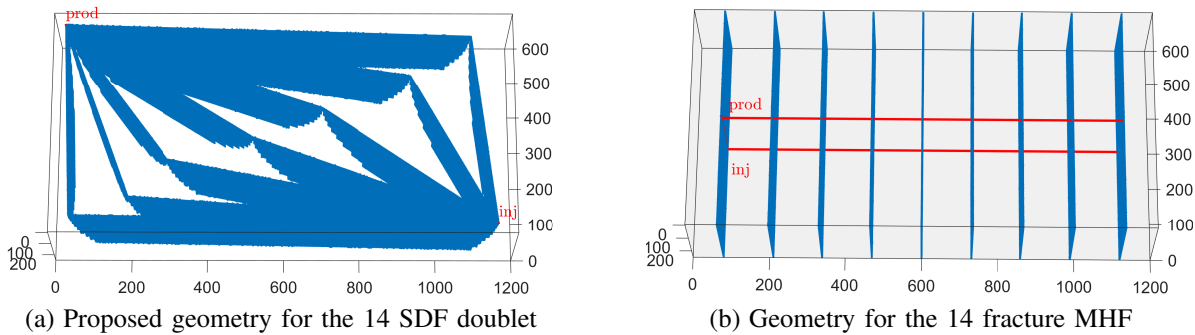


Fig. 11. This figure shows the mesh for an EGS configuration.

number of SDF fractures increases. A corresponding MFHW case with the same total fracture area is also provided to facilitate a reasonable comparison with the state-of-the-art approach for thermal recovery from EGS. Fig. 11(a) presents the mesh for the 14 SDF doublet EGS configuration, whereas Fig. 11(b) presents the mesh for the corresponding multistage fractured horizontal well case.

Fig. 12 presents the cumulative thermal energy, produced fluid temperature, and recovery factor for the SDF doublet and MFHW cases. The cumulative thermal energy shows that the SDF case yields more cumulative thermal energy even though the rates of fluid injection and production from both cases are the same. This is because the temperature of the produced fluid is much higher in the SDF case, as shown in Fig. 12(b). Fig. 12(c) shows that the thermal recovery fraction for the SDF case (57%) is over two times more than in the MFHW case (24%) with the same total fracture surface area. In comparison to the

recovery fraction of 34% from the SDF doublet case in Fig. 9(c), this SDF case with 14 SDFs only yields a 68% increase in the recovery fraction even though it uses more than two times the number of SDFs. This observation underscores the importance of performing numerical simulations to determine the optimum number of SDF fractures to recover a given region of the hot subsurface rock. The flexibility offered by the SDF doublet configurations and the economical analysis of the costs associated with each SDF fracture could be pivotal in the commercial recovery of heat from enhanced geothermal systems.

It is worth noting that the produced fluid temperature of the fourteen SDF doublet case is almost constant for three years, unlike that of the MHF case, which declines quickly from the onset of production. This is because the injected fluid volume is partitioned into fourteen, so the fluid flow rate through the fracture is slow and over a much larger distance in comparison

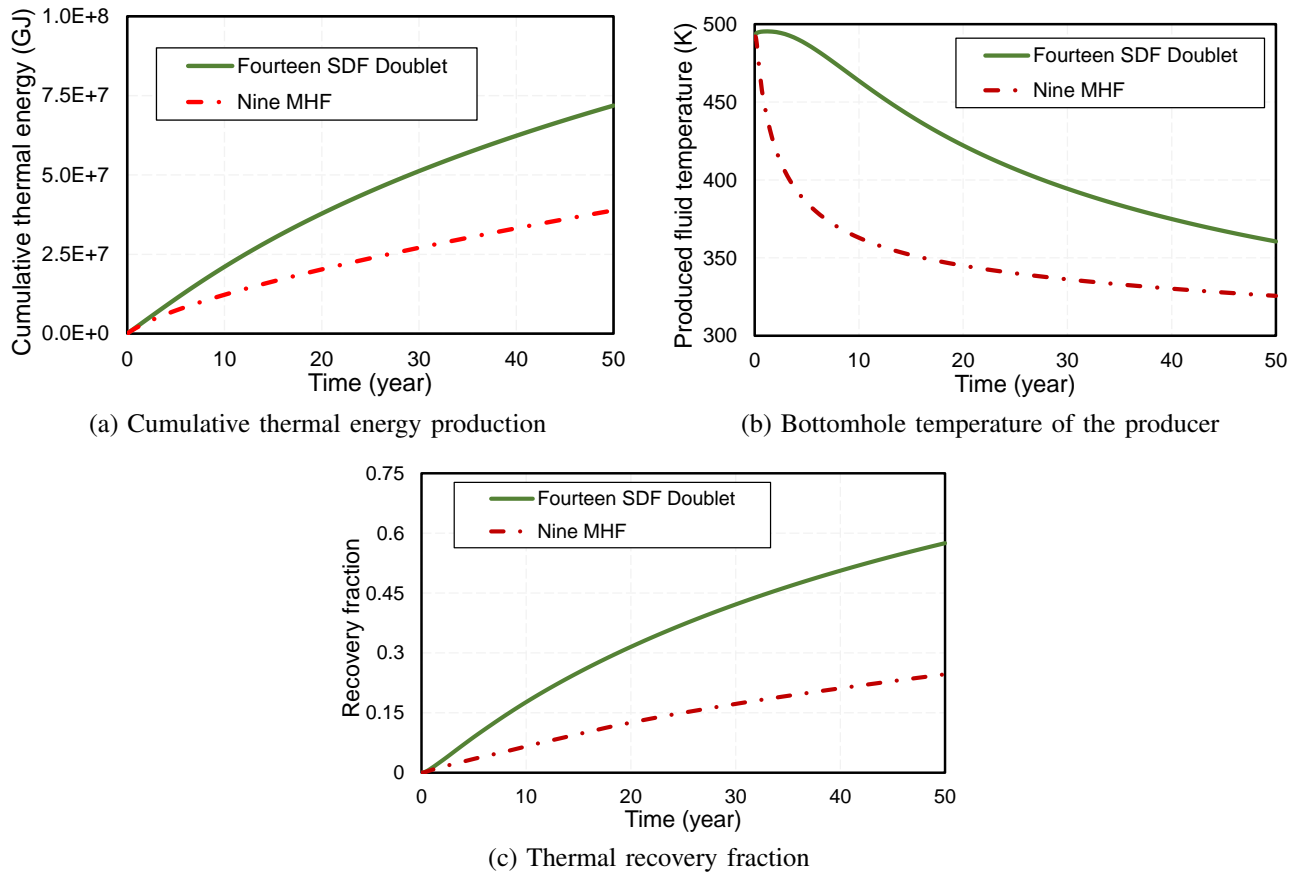


Fig. 12. This figure shows the EGS doublet configuration with 14 SDFs and its corresponding MFHW case.

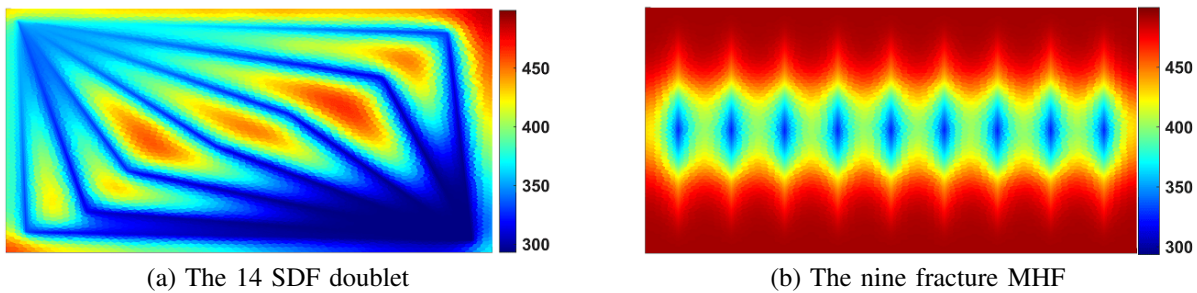


Fig. 13. These profiles show the temperature distribution at the top of the reservoir after simulating the injection and production of water for 50 years.

to the MHF case. This allows the water to be heated close to the initial (volume-weighted average) temperature of the reservoir during the first three years of production. In contrast, the injected cold water in the Nine MHF case is partitioned into nine, and it only interacts with the hot rock over the small distance from the point where the injection well intersects each fracture to the corresponding point where the production well intersects it. So, the producer temperature decreases rapidly as soon as the heat in the area near the fractures is recovered.

Fig. 13 presents the temperature profile for both the SDF doublet and MFHW cases after 50 years of simulated thermal recovery. These profiles again show that the area or volume of the blue-colored region is much more in the SDF case than

in the MFHW case. This indicates that more heat has been recovered from the SDF case than from the MFHW case. As mentioned in the introduction, most enhanced geothermal systems are naturally fractured. So, the next section focuses on studying the effect of NFs on thermal recovery.

6. Thermal recovery in the presence of NFs

To study the effect of NFs on thermal recovery from EGS, ADFNE was used to generate different realizations of NFs. This work used the fully dimensional or explicit fracture model, which involves partitioning each fracture into several fracture cells. Although this approach is very computationally expensive, it is the most accurate approach to model fractured

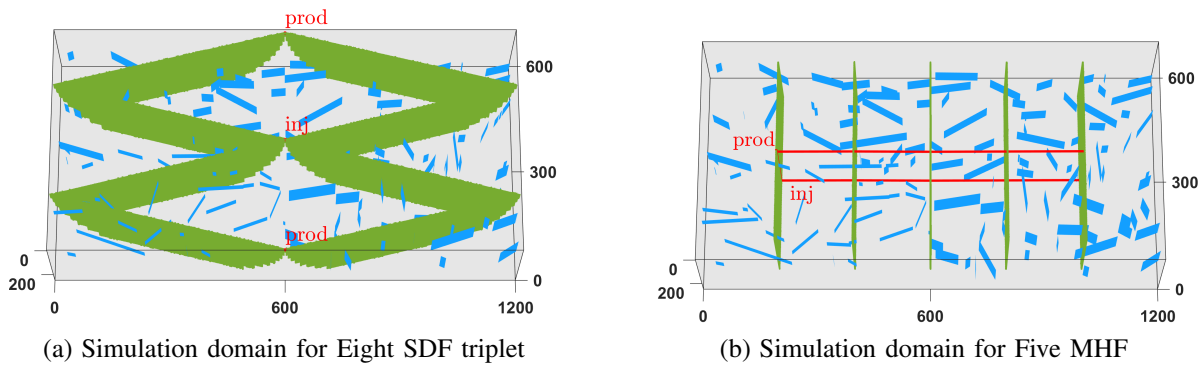


Fig. 14. This figure shows the plot for a naturally fractured reservoir with 160 stochastic NFs.

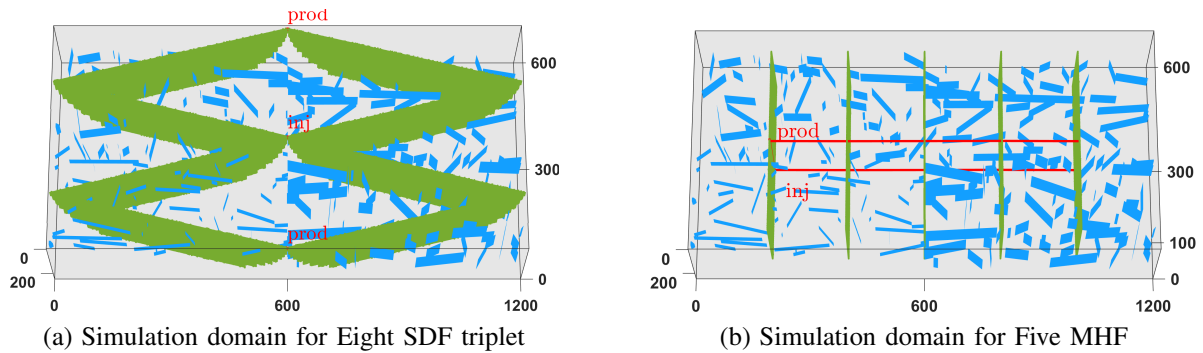


Fig. 15. This figure shows the plot for a naturally fractured reservoir with 375 stochastic NFs.

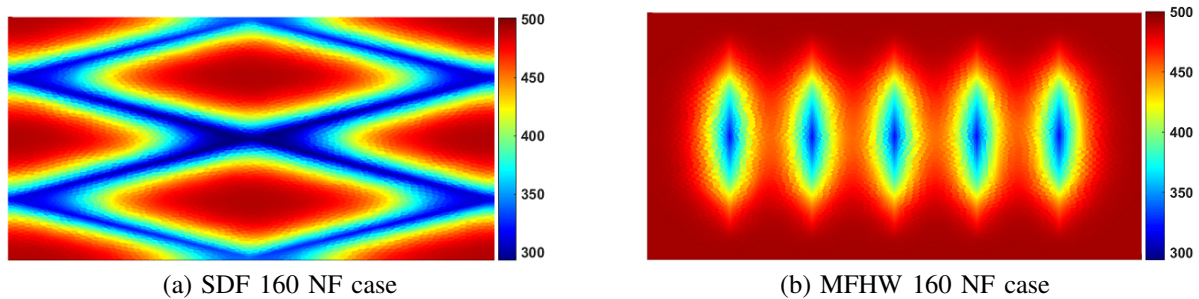


Fig. 16. These profiles show the temperature distribution at the top of the fractured hot rock with 160 NFs, after simulating 50 years of thermal recovery.

reservoirs. The idea is to obtain high-resolution reference solutions, which can be used to validate the application of other fracture models such as discrete fracture models (Karimi-Fard et al., 2004), embedded discrete fracture models (Li and Lee, 2008), pEDFM (Tene et al., 2017; Olorode et al., 2020) in EGS. Fig. 14 presents the mesh for a naturally fractured system with 160 NFs.

In Fig. 14(a), the thermal energy in the naturally fractured domain is recovered using the eight SDF triplet configuration, whereas Fig. 14(b) uses a five MFHW with the same total fracture surface area. To evaluate the effect of increasing the number of NFs, Fig. 15 presents the mesh for a reservoir of the same size but with 375 fractures instead of 160. We also simulated the thermal recovery from this fractured hot rock using the SDF triplet configuration and a corresponding

MFHW case.

Fig. 16 presents the temperature profile after simulating 50 years of thermal recovery from the fractured hot rock with 160 NFs. In the images shown in Figs. 16(a) and 16(b), the first 150 meters from the top of the reservoir domain were clipped. So, these profiles correspond to the plan view of the lower half of the reservoir domain. From the blue-colored regions of the temperature profiles, it is observable that only the NFs connected to the SDF or hydraulic fractures contribute appreciably to the thermal recovery.

Fig. 17 presents the performance plots for the thermal recovery from the naturally fractured systems presented in this section. The results indicate no appreciable difference in all the profiles presented for the MFHW cases with no NF, 160 NFs, and 375 NFs. Although no noticeable difference

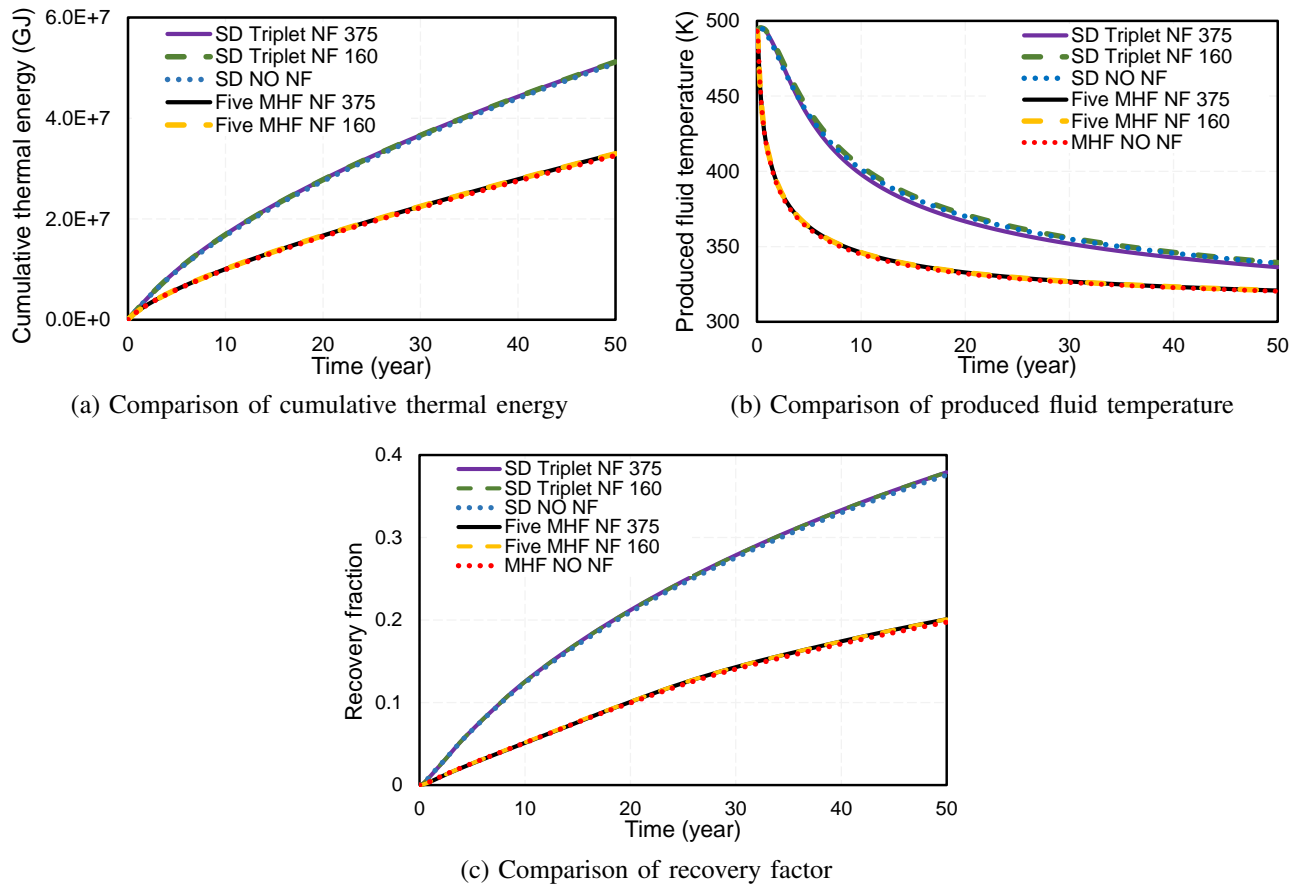


Fig. 17. These profiles show the temperature distribution of natural fracture cases after simulating the injection and production of water for 50 years.

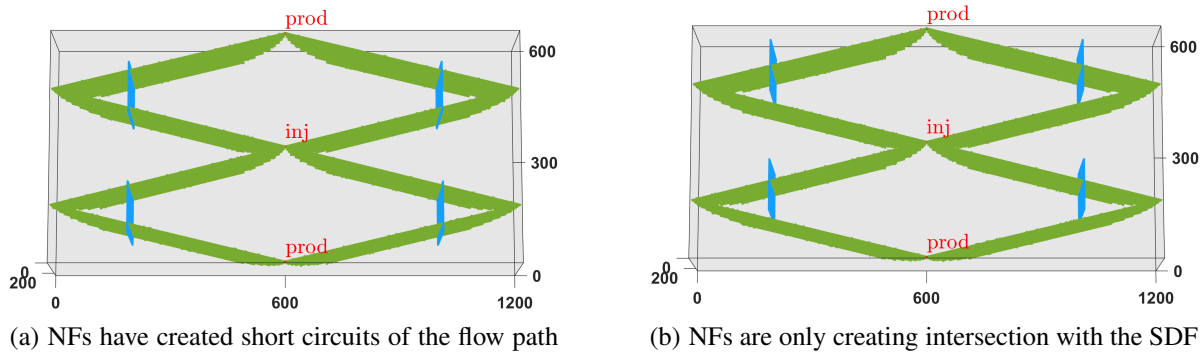


Fig. 18. Simulation domain for the study of short circuit of flow through the natural fracture.

is observed in the cumulative thermal energy and recovery fraction for the SDF cases, a slight difference can be observed in the produced fluid temperature in Fig. 17(b). The SDF case with 160 NFs yielded the highest produced fluid temperature, whereas the SDF case with 375 NFs had a produced fluid temperature that was even lower than the SDF case without NFs. This interesting result highlights the well-known fact that large conductive NFs can short-circuit the produced fluid path. So, a linear increase in the produced fluid temperature is not expected as the number of NFs increases. However, it is worth noting that the recovery fraction for all SDF cases is still

about the same. This implies that the NFs do not curtail the performance of the proposed application of SDF technology in enhanced geothermal systems.

To further investigate the potential of large NFs to short-circuit the desired fluid flow path in SDF EGS, four moderately sized conductive NFs were manually placed in the reservoir domain. In Fig. 18(a), these four NFs are placed in such a way that they short-circuit the desired flow along the path of the intersecting SDFs. In contrast, they were inserted such that they can enhance the thermal recovery in Fig. 18(b). It is worth noting that although the actual location of the NFs

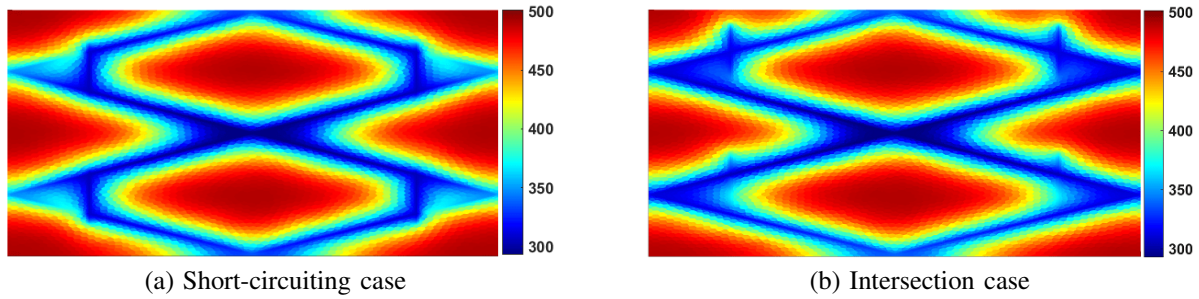


Fig. 19. These profiles show the temperature distribution at the top of the reservoir after simulating the injection and production of water for 50 years.

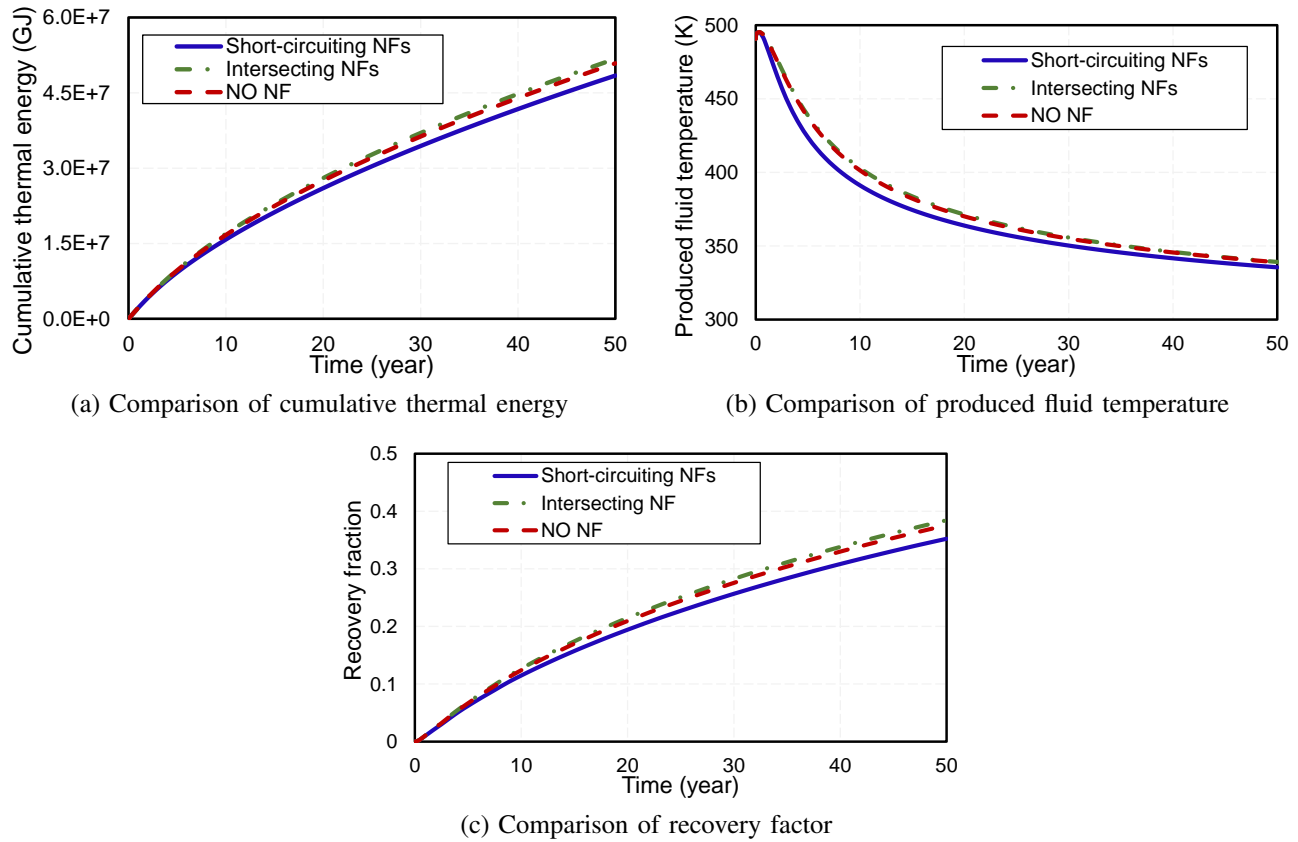


Fig. 20. These profiles show the simulation results of short circuit cases after simulating the injection and production of water for 50 years.

is fixed in the subsurface, their location can be uncertain. So, it is reasonable to simulate the location of these fractures at different points in the domain. Additionally, we did not bother optimizing the location of the natural fracture because the goal is not to show the most optimum configuration, but to point out the fact that the thermal recovery can either be increased or decreased depending on how the SDFs are located relative to the position of known or mapped NFs in the domain.

Fig. 19 presents the temperature profiles after simulating the thermal recovery for 50 years from the two cases shown in Fig. 18. The temperature profile in Fig. 19(a) indicates that the natural fracture short-circuits the regions where the SDF fractures intersect. This reduces the length of the flow path

of the fluid towards the production well and consequently reduces the total surface area of the subsurface rock that the injected water contacts. In contrast, the temperature profile in Fig. 19(b) shows that the total surface area that the injected water contacts increases due to the presence of the natural fracture. So, the natural fracture contributes to an increased thermal recovery instead of curtailing thermal recovery due to the short-circuiting of the desired flow path.

Fig. 20 presents the plots of the cumulative thermal energy, produced fluid temperature, and thermal recovery fraction after simulating heat recovery from the two systems presented in Fig. 18, as well as a case without the four NFs. The results show that the thermal recovery fraction is lower in the case of

Table 3. Parameters used in the Utah Forge case study.

Parameters	Value	Unit
Matrix permeability	1e-18	m ²
Matrix porosity	0.001	/
Fracture permeability	9.8692e-12	m ²
Fracture porosity	0.0015	/
Fracture spacing in MHF	200	m
Fracture aperture	0.05	m
Total fracture volume	6.96e6	m ³
Reservoir dimensions	1200 × 600 × 250	m ³
Initial reservoir pressure	2.8e7	Pa
Initial reservoir temperature	536	K
Injected fluid temperature	293	K
Constant injection rate	0.069	m ³ /s
Constant producer bhp	2.5e7	Pa
Rock thermal conductivity	3.05	W/(m·K)
Rock density	2,750	Kg/m ³
Heat capacity	790	J/(Kg·K)
Fluid thermal conductivity	0.6	W/(m·K)
Fluid heat capacity	4,200	J/(Kg·K)
Coefficient of thermal expansion	2.07e-4	K ⁻¹
Fluid compressibility	2.5e-12	Pa ⁻¹
Fluid density	1,000	Kg/m ³
Fluid viscosity	5e-4	Pa·s

the short-circuiting NFs. In contrast, it is slightly higher when the NFs are placed in a somewhat different location relative to the SDFs.

Although the location of the NFs is fixed in the subsurface, the flexibility in the SD doublet fracture configurations can be leveraged to design the path of the SDFs so that they improve the thermal recovery instead of decreasing it due to a short-circuiting of the desired flow path. In contrast, the lack of control over the path of propagating hydraulic fractures makes it practically impossible to design MFHWs to take advantage of large NFs or faults, even when we know their location and orientation from image logs, and seismic and micro-seismic data. Furthermore, performing a similar study of the role of known large NFs on MFHWs is considered unnecessary because there is no technology to guarantee that any modeled hydraulic fracture configurations (that intersect the NFs at specific points) can be created in the subsurface.

7. Evaluation of the use of SDFs in the Utah FORGE

This section discusses our numerical studies of the applicability of the proposed model by simulating a system representative of the Utah FORGE project. To this end, we

obtained the model parameters from topical reports from the Utah FORGE Phase 2C (Moore et al., 2019), and these are summarized in Table 3. The thermal recovery from the representative Utah FORGE subsurface rock is modeled using the proposed SD configuration and the current approach, which is based on two pairs of parallel horizontal/deviated wells.

The images in Figs. 21(a) and 21(b) show the simulation domain for the SDF and MFHW cases, respectively. The total fracture surface areas in both cases are the same to ensure a reasonable comparison of their thermal recoveries. Considering that the Utah FORGE reservoir is naturally fractured, ADFNE was used to generate a stochastic natural fracture network with 500 NFs.

Fig. 22 presents the simulated temperature profiles for applying the SDF and MFHW technologies in a representative Utah FORGE reservoir. These profiles indicate that the blue-colored region of the SDF temperature profile is much larger than the correspondingly colored region of the MFHW profile. The larger volume of these regions with lower temperatures after 50 years of simulated thermal recovery also confirms that the proposed technology can recover more heat from the hot fractured rocks in the subsurface.

The plots of the cumulative thermal energy, produced fluid

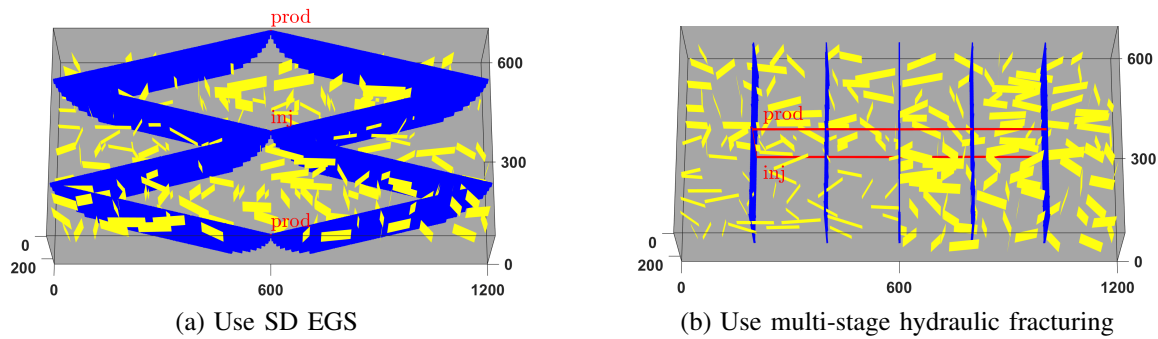


Fig. 21. These profiles show the temperature distribution in Utah Forge with 500 NFs after simulating the injection and production of water for 50 years.

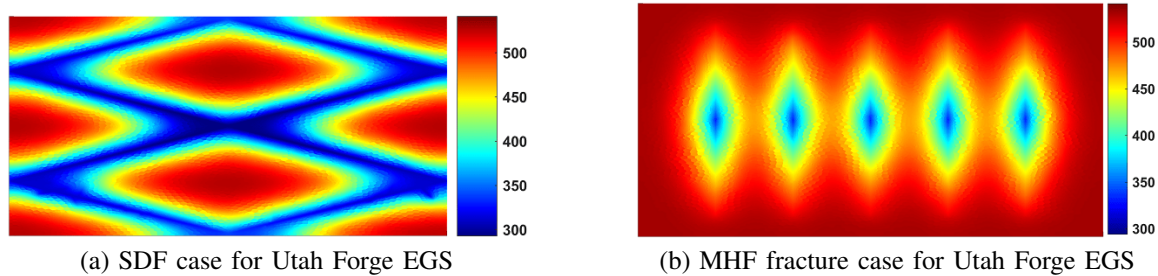


Fig. 22. These profiles show the temperature distribution at the top of the reservoir after simulating the injection and production of water for 50 years.

temperature, and thermal recovery fraction are given in Figs. 23(a), 23(b), and 23(c), respectively. These results show that the thermal recovery fraction of the proposed technology is 50% higher than that of the state-of-the-art technology, which is currently being used in the Utah FORGE project. As explained in the previous section, the difference in the cumulative thermal energy is smaller because the same volume of water is injected and produced in both cases. However, the produced fluid temperature is considerably higher in the SDF case, resulting in its much higher thermal recovery fraction.

8. Conclusions

This paper presents high-resolution numerical simulation studies of the performance of the state-of-the-art MFHW approach to recover heat from EGS compared to our proposed approach that uses slot-drilled fractures. The performance plots and temperature profiles for all the simulated cases show that the proposed approach significantly outperforms the MFHW approach to different degrees, depending on the configuration of the SDF system and the model parameters. The proposed technology yields a 50% higher thermal recovery fraction for the representative Utah FORGE field case simulated. Other conclusions based on the various cases simulated can be summarized as follows:

- The SDF doublet appears to be the most promising of the SDF EGS configurations proposed because it uses the fewest wells per unit reservoir volume, and its recovery is only slightly lower than that of the corresponding SDF triplet configuration. This, coupled with the flexibility it

offers regarding the optimization of the number of SDFs per unit volume, makes it a lower-cost, higher-profit, and more flexible alternative to the proposed SDF triplet configuration.

- The results from the natural stochastic fracture systems studied indicates that the contribution of NFs to heat recovery is minimal. However, the SDF doublet configuration can be designed to avoid being short-circuited by large NFs or faults known to be present in the hot rock.
- The control over the location, size, orientation, and aperture of the slot-drilled fractures provides more reliability in terms of comparing the system modeled to the actual EGS in the subsurface. In contrast, the actual MFHW system could be a lot less efficient than the simulated system because of the lack of control over the size, orientation, and geometry of the hydraulic fractures. There is also no guarantee that the injection and production wells will intersect all the hydraulic fractures.

For completeness, it is worth clarifying that the single-phase formulation used in this work implies that the results are only directly applicable to low-enthalpy geothermal reservoirs. However, we do not expect the conclusions on the performance of the proposed technology relative to the state-of-the-art approach to change due to multiphase flow and the presence of salts and other impurities. Mechanical deformation can lead to a reduction in fracture conductivity over time if the pore pressure decreases considerably, but the continued injection of water during this process, as well as the availability of proppants, make this relatively less important.

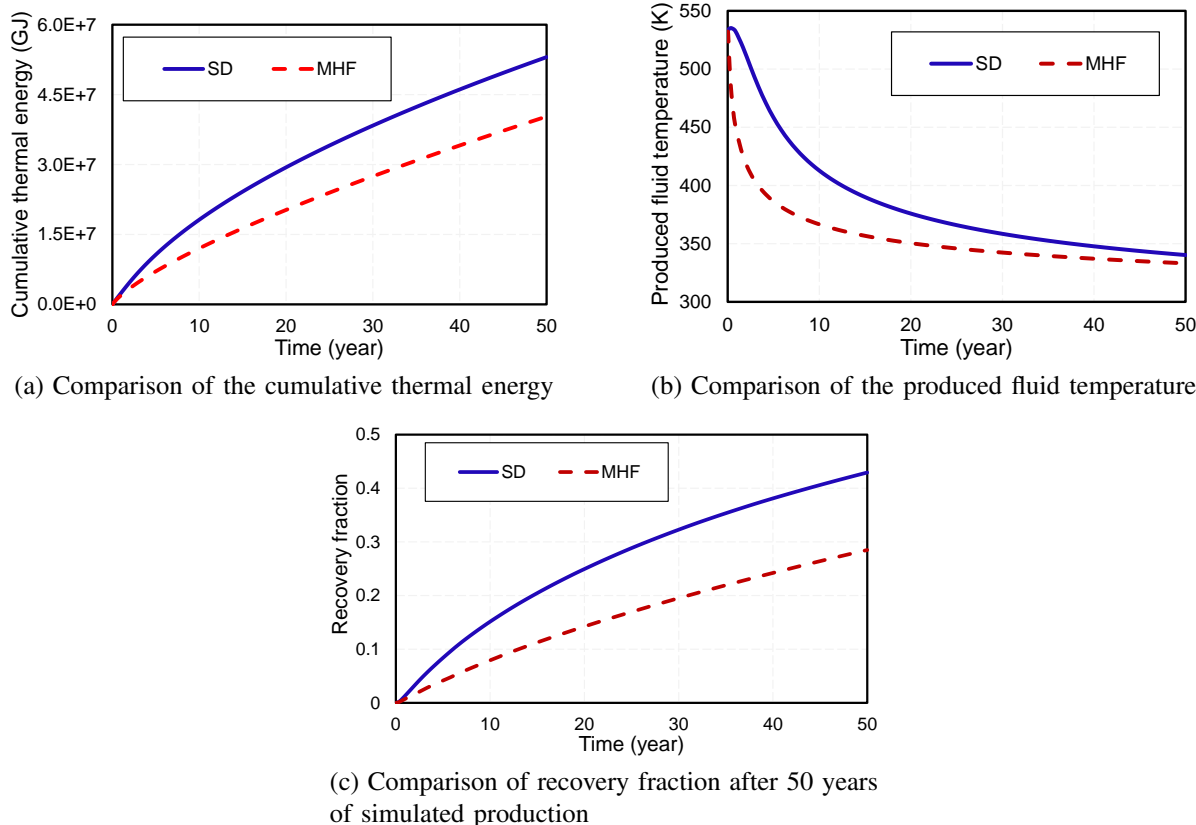


Fig. 23. All profiles presented in this figure show that the proposed SDF system significantly outperforms the multistage fractured horizontal well.

Acknowledgements

This work was facilitated using the software packages available in the Craft and Hawkins Department of Petroleum Engineering at Louisiana State University (LSU) and the computational resources at the LSU Center for Computation and Technology (CCT).

Supplementary file

<https://doi.org/10.46690/ager.2024.04.04>

Conflict of interest

The authors declare no competing interest.

Open Access This article is distributed under the terms and conditions of the Creative Commons Attribution (CC BY-NC-ND) license, which permits unrestricted use, distribution, and reproduction in any medium, provided the original work is properly cited.

References

- Aghahosseini, A., Breyer, C. From hot rock to useful energy: A global estimate of enhanced geothermal systems potential. *Applied Energy*, 2020, 279: 115769.
- Alghalandis, Y. *DFNE Practices with ADFNE*. Alghalandis Computing, Toronto, Ontario, Canada, 2018.
- Amer, H., Olorode, O. Numerical evaluation of a novel slot-drill enhanced oil recovery technology for tight rocks. *SPE Journal*, 2022, 27(4): 2294-2317.
- Asai, P., Panja, P., McLennan, J., et al. Performance evaluation of enhanced geothermal system (egs): Surrogate models, sensitivity study and ranking key parameters. *Renewable Energy*, 2018, 122: 184-195.
- Batchelor, A. S. Brief summary of some geothermal related studies in the United Kingdom. Paper Presented at the second NATO-CCMS meeting on dry hot rock geothermal energy, Los Alamos, NM, USA, 28 June, 1977.
- Berge, R. L., Klemetsdal, Ø., Lie, K.-A. Unstructured voronoi grids conforming to lower dimensional objects. *Computational Geosciences*, 2019, 23: 169-188.
- Berge, R. L., Klemetsdal, Ø., Lie, K.-A. Unstructured PEBI grids conforming to lower-dimensional objects, in *Advanced Modeling with the MATLAB Reservoir Simulation Toolbox*, edited by K.-A. Lie and O. Møyner, Cambridge University Press, Cambridge, pp. 3-45, 2021.
- Carter, E. Novel concepts for unconventional gas development of gas resources in gas shales, tight sands and coalbeds. Final report RPSEA Subcontract, 2009.
- Carter Jr, E. E. Method and apparatus for increasing well productivity. US 9732561, 2017.
- Collignon, M., Klemetsdal, Ø. S., Møyner, O., et al. Evaluating thermal losses and storage capacity in high-temperature aquifer thermal energy storage (HT-ATES) systems with well operating limits: Insights from a study-

- case in the Greater Geneva Basin, Switzerland. *Geothermics*, 2020, 85: 101773.
- Collignon, M., Klemetsdal, Ø. S., Møyner, O. Simulation of geothermal systems using MRST, in *Advanced Modeling with the MATLAB Reservoir Simulation Toolbox*, edited by K.-A. Lie and O. Møyner, Cambridge University Press, Cambridge, pp. 491-514, 2021.
- Farrar, R. B., Mayercheck, W. D., Bockosh, G. R. Method of mining a mineral deposit seam. US 5033795, 1991.
- Franco, A., Donatini, F. Methods for the estimation of the energy stored in geothermal reservoirs. *Journal of Physics: Conference Series*, 2017, 796: 012025.
- Gilman, J. R., Kazemi, H. Improvements in simulation of naturally fractured reservoirs. *SPE Journal*, 1983, 23(4): 695-707.
- Gong, F., Guo, T., Sun, W., et al. Evaluation of geothermal energy extraction in Enhanced Geothermal System (EGS) with multiple fracturing horizontal wells (MFHW). *Renewable Energy*, 2020, 151: 1339-1351.
- Hurd, R. L. Method and apparatus for deep mining using chain driven in fixed direction. US 4232904, 1980.
- Jung, Y., Pau, G. S. H., Finsterle, S., et al. Tough3 user's guide, version 1.0. 2021.
- Karimi-Fard, M., Durlofsky, L. J., Aziz, K. An efficient discrete-fracture model applicable for general-purpose reservoir simulators. *SPE Journal*, 2004, 9(2): 227-236.
- Kim, J.-G., Deo, M. D. Finite element, discrete-fracture model for multiphase flow in porous media. *AIChE Journal*, 2000, 46(6): 1120-1130.
- Klemetsdal, Ø., Andersen, O., Krogstad, S., et al. Modelling and optimization of shallow underground thermal energy storage. *Geoenergy*, 2023, 1(1): geoenergy2023-005.
- Lie, K.-A. An Introduction to Reservoir Simulation Using MATLAB/GNU Octave: User Guide for the MATLAB Reservoir Simulation Toolbox (MRST). Cambridge, UK, Cambridge University Press, 2019.
- Lie, K.-A., Møyner, O. *Advanced Modeling with the MATLAB Reservoir Simulation Toolbox*. Cambridge, UK, Cambridge University Press, 2021.
- Li, L., Lee, S. H. Efficient field-scale simulation of black oil in a naturally fractured reservoir through discrete fracture networks and homogenized media. *SPE Reservoir Evaluation & Engineering*, 2008, 11(4): 750-758.
- March, R., Maier, C., Doster, F., et al. A unified framework for flow simulation in fractured reservoirs, in *Advanced Modeling with the MATLAB Reservoir Simulation Toolbox*, edited by K.-A. Lie and O. Møyner, Cambridge University Press, Cambridge, pp. 454-490, 2021.
- Moore, J., Simmons, S., McLennan, J., et al. Utah forge: Phase 2c topical report. Energy and Geoscience Institute at the University of Utah, 2019.
- Oduowo, T. O. Numerical simulation study to investigate expected productivity improvement using the "Slot-Drill" completion. Texas, Texas A & M University, 2012.
- Olorode, O. M., Freeman, C. M., Moridis, G. J., et al. High resolution numerical modeling of complex and irregular fracture patterns in shale-gas reservoirs and tight gas reservoirs. *SPE Reservoir Evaluation & Engineering*, 2013, 16(4): 443-455.
- Olorode, O., Wang, B., Rashid, H. U. Three-dimensional projection-based embedded discrete-fracture model for compositional simulation of fractured reservoirs, *SPE Journal*, 2020, 25(4): 2143-2161.
- Olorode, O., Wang, B., Rashid, H. U. Numerical modeling of fractured unconventional oil, in *Advanced Modeling with the MATLAB Reservoir Simulation Toolbox*, edited by K.-A. Lie and O. Møyner, Cambridge University Press, Cambridge, pp. 409-453, 2021.
- Pruess, K., Narasimhan, T. N. A practical method for modeling fluid and heat flow in fractured porous media. *SPE Journal*, 1982, 25(1): 14-26.
- Rao, X., Liu, Y. A numerical modeling method of fractured reservoirs with embedded meshes and topological fracture projection configurations. *Computer Modeling in Engineering & Sciences*, 2022, 131(3): 1403-1429.
- Rao, X., Xin, L., He, Y., et al. Numerical simulation of two-phase heat and mass transfer in fractured reservoirs based on projection-based embedded discrete fracture model (pEDFM). *Journal of Petroleum Science and Engineering*, 2022, 208: 109323.
- Rashid, H. U., Abbasi, B., Mohanty, M. Performance optimization of an EGS in Nevada using DFN models. Paper ARMA-DFNE-18-0761 Presented at the 2nd International Discrete Fracture Network Engineering Conference, Seattle, Washington, USA, 20-22 June, 2018.
- Rashid, H. U., Olorode, O. A continuous projection-based EDFM model for flow in fractured reservoirs. *SPE Journal*, 2024, 29(1): 476-492.
- Ṭene, M., Bosma, S. B., Kobaisi, M. S. A., et al. Projection-based Embedded Discrete Fracture Model (pEDFM). *Advances in Water Resources*, 2017, 105: 205-216.
- Tester, J. W., Anderson, B. J., Batchelor, A., et al. The future of geothermal energy. Massachusetts Institute of Technology, 2006.
- Warren, J. E., Root, P. J. The behavior of naturally fractured reservoirs. *SPE Journal*, 1963, 3(3): 245-255.
- Wong, D., Doster, F., Geiger, S. Embedded discrete fracture models, in *Advanced Modeling with the MATLAB Reservoir Simulation Toolbox*, edited by K.-A. Lie and O. Møyner, Cambridge University Press, Cambridge, pp. 375-408, 2021.